Redox Biology 46 (2021) 102114

Contents lists available at ScienceDirect

Redox Biology

journal homepage: www.elsevier.com/locate/redox

Cardioprotective effect of MLN4924 on ameliorating autophagic flux impairment in myocardial ischemia-reperfusion injury by Sirt1

Ji Zhang [a,b,1,*], Jing Cui [c,1], Fei Zhao [c], Longhua Yang [c], Xueli Xu [c], Yangyang Shi [c], Bo Wei [c,**]

[a] Department of Pharmacy, The First Affiliated Hospital of Zhengzhou University, Zhengzhou, 450052, PR China
[b] Henan Key Laboratory of Precision Clinical Pharmacy, Zhengzhou University, Zhengzhou, 450052, PR China
[c] Key Laboratory of Advanced Pharmaceutical Technology, Ministry of Education of China, School of Pharmaceutical Sciences, Zhengzhou University, No. 100 Kexue Avenue, Zhengzhou, Henan, 450001, PR China

ARTICLE INFO

Keywords:
MLN4924
Autophagic flux
Sirt1
Myocardial ischemia/reperfusion

ABSTRACT

Neddylation is essential for cardiomyocyte survival in the presence of oxidative stress, and it participates in autophagy regulation. However, whether MLN4924—an inhibitor of neddylation—exerts cardioprotective effects against myocardial ischemia/reperfusion (MI/R) remains unknown. In the present study, MLN4924 exerted strong cardioprotective effects, demonstrated by significantly elevated cell viability, a decreased LDH leakage rate, and improved cell morphology following H_2O_2-induced injury *in vitro*. MLN4924 also markedly decreased the serum myocardial zymogram level, ameliorated cardiac histopathological alterations, and alleviated left ventricular contractile dysfunction, thus limiting the cardiac infarct size *in vivo* compared with those in MI/R mice. Amazingly, such action of MLN4924 was abrogated by a combined treatment with the autophagic flux inhibitor, chloroquine. The mRFP-GFP-LC3 assay illustrated that MLN4924 restored the defective autophagic flux via enhancing the autolysosome formation. Notably, the expression levels of Rab7 and Atg5 were markedly up-regulated in MLN4924 treated cells and mice subjected to H_2O_2 or MI/R, respectively, while knockdown of Sirt1 in cells and heart tissue largely blocked such effect and induced autophagosome accumulation by inhibiting its fusion with lysosomes. Transmission electron microscopic analysis, histopathological assay and TUNEL detection of the heart tissues showed that the absence of Sirt1 blocked the cardioprotective effect of MLN4924 by further exacerbating the impaired autophagic flux during MI/R injury *in vivo*. Taken together, MLN4924 exhibited the strong cardioprotective action via restoring the impaired autophagic flux in H_2O_2-induced injury *in vitro* and in MI/R mice. Our work implicated that Sirt1 played a critical role in autophagosome clearance, likely through up-regulating Rab7 in MI/R.

1. Introduction

Timely reperfusion is required to prevent cardiomyocyte loss and limit the infarct size (IS) against myocardial infarction, but the accompanying myocardial ischemia/reperfusion (MI/R) injury is associated with oxidative stress and cell death [1].

Autophagy, a dynamic cellular biological process from the formation of autophagosome, autophagosome-lysosome fusion to final degradation, is closely associated with both oxidative stress and cell death. Noteworthy, cardiac autophagy adapts to nutrient and oxygen deprivation during myocardial ischemia, and mediates cell death during reperfusion injury in the heart [2]. Recently and importantly, researchers have further demonstrated that the impaired autophagic flux during the phase of reperfusion leads to the accumulation of autophagosomes, which is detrimental to cardiomyocyte survival during reperfusion [3–5]. Furthermore, a decline in autophagic flux is closely associated with reactive oxygen species (ROS) accumulation of ROS and mitochondrial damage, which itself is a source of ROS [6,7].Therefore, improvement of the autophagic flux and decrease of ROS are the current targets for the development of cardiovascular disorder drugs, especially for MI/R.

Post-translational Neddylation is a process of adding the ubiquitin-like molecule NEDD8 to the target proteins, and plays a critical role in the regulation of protein function. MLN4924, a specific NAE1 inhibitor, has recently gained a lot of attention in a variety of diseases due to its

* Corresponding author. The First Affiliated Hospital of Zhengzhou University, Department of Pharmacy, Zhengzhou, Henan, 450052, PR China.
** Corresponding author. Zhengzhou University School of Pharmaceutical Sciences, Zhengzhou, Henan, 450001, PR China.
E-mail addresses: fcczhangj@zzu.edu.cn (J. Zhang), weibozz101@163.com (B. Wei).
[1] These authors contributed equally to this work.

https://doi.org/10.1016/j.redox.2021.102114
Received 12 July 2021; Received in revised form 19 August 2021; Accepted 19 August 2021
Available online 24 August 2021

Abbreviations

AAR	area at risk
ADV	adenoviral vector
AST	aspartate transaminase
ATCC	american type culture collection
CETSA	cellular thermal shift assay
CK-MB	creatine kinase-mb
CRLs	cullin-ring e3 ubiquitin ligases
DHE	dihydroethidium
ECG	electrocardiogram
EF	ejection fraction
FS	fractional shortening
GSH	glutathione
HE	hematoxylin-eosin
H_2O_2	hydrogen peroxide
LAD	left anterior descending
LDH	lactate dehydrogenase
MDA	malondialdehyde
MI/R	ischemia/reperfusion injury
MOI	multiplicity of infection
PBS	phosphate-buffered saline
SOD	superoxide dismutase
TEM	transmission electron microscopy
TUNEL	terminal deoxynucleotidyl transferase-mediated dutp nick end labeling

effect on oxidative stress and inflammation, including cancer, neurological disorders, and pulmonary fibrosis [8–10]. Meanwhile, Luo and his colleagues have recently discovered that MLN4924 could trigger an intact autophagic flux in MLN4924-treated cancer cells [11]. Recently, Neddylation inhibition by MLN4924 has been demonstrated to increase autophagic flux in vascular smooth muscle cells and in the mouse brain tissue, respectively [12,13]. Additionally, MLN4924 treatment alone does not impair autophagic flux in mouse hearts [13]. However, its potential effects on MI/R and cardiac autophagic flux deficiency remain largely unknown. We, therefore, investigated the effects of MLN4924 on MI/R and cardiac autophagic flux using cultured H9c2 cells subjected to H_2O_2 exposure and a mice model of MI/R.

2. Materials and methods

2.1. Materials

MLN4924 (purity>98%) was purchased from MedChemExpress Ltd., New Jersey, USA. Creatine Kinase-MB (CK-MB), Aspartate Transaminase (AST), Lactate Dehydrogenase (LDH), Superoxide Dismutase (SOD), Malondialdehyde (MDA) and Glutathione (GSH) Commercial Kits were obtained from Jiancheng Institute of Biotechnology (Nanjing, China). Terminal Deoxynucleotidyl Transferase-Mediated Dutp Nick End Labeling (TUNEL) BrightRedApoptosis Detection Kit was purchased from Vazyme Biotech (Nanjing, China). All the other reagents used were of analytical grade.

2.2. Cell culture and treatment

H9c2 embryonic rat heart-derived myoblasts purchased from American Type Culture Collection (ATCC, Shanghai, China) (CRL-1446) were cultured in Dulbecco's Modified Eagle Media: Nutrient Mixture F-12 (DMEM/F12) with 10% FBS (GIBCO, Carlsbad, California, USA) and 100IU·mL^{-1} penicillin and 100 μg·mL^{-1} streptomycin at 37 °C in a humidified atmosphere of 5% CO_2. Cells were synchronized by serum starvation before stimulated with MLN4924 or hydrogen peroxide (H_2O_2). Cells were fed every 2–3 days and sub-cultured when they reached 70–80% confluence.

2.3. MLN4924 and H_2O_2 treatment

The effect of MLN4924 was investigated in H9c2 cells treated with H_2O_2 as described [14]. Briefly, when cells reached 70–80% confluence, MLN4924 was dissolved in cell culture media containing 0.1% DMSO. For the experiments performed in the presence of MLN4924, the compound was added to cells, 24 h prior to hydrogen peroxide treatment, followed by incubation for another 2 h. Cells of the control group *in vitro* were treated with DMSO at 0.1% (v/v). The exact group size for each experimental group *in vitro* is 5.

2.4. Adenoviral-mediated gene transfer

Sense or antisense Sirt1 adenoviruses (Ad.Sirt1 or Ad.Sirt1-AS) or control Ad.GFP were obtained from Biocan BioTECH (Shenzhen, China). Adenoviruses were amplified in HEK293 cells, purified with ViraKit from Virapur and tittered, according to the standard procedure of AdenoXTM rapid titer kit from BIOMIGA. After 2 h of plating, H9c2 cells were infected with sense or antisense Sirt1 adenoviruses (ie. Ad.Sirt1 or Ad.Sirt1-AS) or control Ad.GFP at a multiplicity of infection (MOI) of 400 for 2 h before the addition of a suitable volume of complete DMEM medium. The efficiency of adenoviral gene transfection was detected in cultured H9c2 cells by immunofluorescent signal through fluorescence microscopy (Nikon Eclipse Ti–S, Nikon Ltd, Japan). Nearly 100% of H9c2 cells appeared infected at 400 MOI by 48 h. The cell phenotype and morphology remained similar among non-infected and adenoviral-infected groups after 48 h of infection. The cells were then treated with MLN4924 or H_2O_2 for indicated time, washed with PBS and harvested for quantitative immunoblotting, or used in the experiments outlined in the results.

2.5. Cell viability and LDH assays

The MTT assay was performed to evaluate the H9c2 cells viability after MLN4924 and H_2O_2 treatment. Briefly, the H9c2 cells were seeded in 96-well plates (200μL/well) at a density of 5000 cells/well were grown at 37 °C for 24 h until confluence reached ≥80%. Then cells were starved for 12 h in DMEM/F12 or DMEM supplemented with 0.5% FBS. After serum starvation, H9c2 cells were cultured with different concentration of MLN4924 (0.05, 0.1, 0.33, 0.5 and 1 μM) for 24 h. To evaluate the protective effects of MLN4924, H9c2 cells were cultured with different concentration of MLN4924. Then, cells were exposed to 250 μM H_2O_2 for 2 h. On the other hand, after treatments (exposed to 2 h of H_2O_2 with or without MLN4924 and CQ (20 μM for 24 h; MedChem Express, USA) in different groups), H9c2 cells in different groups were treated with MTT solution incubated for 4 h at 37 °C in the dark. Model groups were incubated under the same conditions, while cells in control groups were treated with the same volume of phosphate-buffered saline (PBS). After the indicated time, cell viability was evaluated by MTT assay.

The lactate dehydrogenase (LDH) leakage assay was used to assess cytotoxicity after different treatments. The LDH release rate was measured using the cytotoxicity detection kit, according to the manufacturer's instructions (C0016, Beyotime, Shanghai, China) and quantified by absorbance at 490 nm using a BioTek plate reader. Results were normalized to the control group, the amount of LDH release of which was considered as 100%.

2.6. Detection of ROS

Intracellular levels of ROS were assessed using conversion of non-fluorescent dihydroethidium (DHE) to fluorescent ethidium bromide [14,15]. Briefly, H9c2 cells were plated in a 6-well plate (2.5×10^5 cells/well) and incubated with the designated doses of MLN4924 and H_2O_2. Cells were then washed in PBS and incubated with 5 μM DHE at 37 °C for 30 min according to the manufacturer's instructions. Ethidium fluorescence (excitation at 495 nm, emission at 529 nm) was examined by flowcytometry (Accuri C6, BD) immediately. Ten thousand cells were collected and analyzed. The superoxide anion levels were calculated by the FlowJo software. Additionally, morphological analysis was performed through fluorescence microscopy (Nikon Eclipse Ti–S, Nikon Ltd, Japan). For calculation of relative changes in ROS level, values of individual samples were divided by the mean value of samples from the Ad.GFP control group.

2.7. Evaluation of fluorescent LC3 puncta

Cells cultured on coverslips were transfected with adenovirus of tandem fluorescent mRFP-GFP-LC3 (Hanbio, Inc., Shanghai, CN) (MOI = 800), a specific marker for autophagosome formation. After adenoviral transfection for 48 h, cells were fixed with 4% paraformaldehyde after treatment with H_2O_2 or MLN4924. Images of the cells were obtained from the confocal laser scanning microscope (Nikon, A1 PLUS, Tokyo, Japan) and analyzed using the Image J Software. Cells were detected with green (GFP) or red (mRFP) fluorescence. Autophagosomes are yellow puncta and autolysosomes are only red puncta in merged images due to the acidic lysosomal compartment. Autophagic flux was determined by increased percent of only red puncta in the merged images. The transfection efficiency was more than 90%, and the subsequent transfection-induced cell death was less than 10%.

2.8. Molecular docking studies

To explore the possible binding mode of protein Sirt1 and compound MLN4924, molecular docking between them was performed using MOE software. The crystal structure of Sirt1 complexing with its classic resveratrol (PDB ID = 5BTR) was obtained from the RCSB Protein Data Bank (http://www.pdb.org).

2.9. Cellular thermal shift assay (CETSA)

CETSA was performed according to previous research. Cells were seeded in cell culture dishes (100 mm) and treated with 20 μM MLN4924 or 1% DMSO for 4 h at 37 °C. In short, cells were collected and heated individually at different temperatures (42, 43, 46, 50, 55, 59, 62) for 10 min. Then, the samples were centrifuged, and the obtained cells were analyzed by Western blot.

2.10. Animals

All studies involving animals were approved by the Ethical Committee of Zhengzhou University and were in accordance with the ARRIVE guidelines for reporting experiments involving animals [16,17]. Specific pathogen free (SPF) male C57/BL-6 mice weighing 20–25 g were purchased from Beijing Vital River Laboratory Animal Technology Co. Ltd., were used for *in vivo* experiments. 6 mice/cage were housed based on standard diurnal lighting conditions (12 h/12 h) at a controlled ambient temperature of 25 ± 2 °C for 7 days before the experiment. All efforts were made to minimize the suffering of the animals and the number of animals needed to obtain reliable results based on the rules of the replacement, refinement or reduction (the 3Rs).

2.11. Cardiac gene transfer

All of mice were anesthetized with 2–3% isoflurane and underwent a left thoracotomy to expose the heart. 30 μl of recombinant adenovirus (Ad-Sirt1-AS and Ad-GFP) (1×10^{11} pfu) were injected with a Hamilton precision syringe directly into the anterior wall of the left ventricle (LV) from the apex to the base [18,19]. Thereafter, air was evacuated from the thoracic cavity, and the chest was closed. Three days after injection, myocardial I/R model was performed. In a preliminary experiment, we confirmed using Western blot that adenoviral vectors (ADV) express in the infarcted area using Western blot.

2.12. Preparation of mice myocardial I/R model

Mice were anesthetized with 2–3% isoflurane inhalation in an inducing chamber and the adequacy of anesthesia was monitored by the disappearance of the pedal withdrawal reflex [20]. Thereafter, a left thoracotomy was performed to expose the heart and the left anterior descending (LAD) was ligated (no ligation for sham) for 30 min followed by 24 h of reperfusion as previously described [21,22]. The MLN4924 (3 or 6 mg/kg) was directly dissolved in normal saline (NS) containing 0.01%DMSO at 37 °C as described elsewhere and administrated subcutaneously (s.c.) once per day for 7 days before MI/R surgery. The dosage of MLN4924 was designed according to the previous work and our preliminary study [23]. The same amount of NS containing 0.01% DMSO was administrated in Sham mice as vehicle.

2.13. Study design and experimental protocols

All mice were randomly assigned into 5 groups (Sham, MI/R, ML + MI/R, MH + MI/R, and MI/R + MH + Ad.Sirt1-AS, n = 16 for each group). ML refers to the low-dosage of MLN4924 (3 mg/kg) treatment, while MH means the high-dosage of MLN4924 (6 mg/kg). We performed the intramyocardial injection of ADV expressing anti-sense Sirt1 or GFP, combined with the MLN4924 administration (6 mg/kg once per day, for 7 days). On the 7th day, heart functions were assessed by echocardiography, as well as the myocardial ischemia/reperfusion model was performed. Mice were sacrificed after reperfusion for 24 h for further analyses.

2.14. Electrocardiogram (ECG)

Electrocardiographic recordings were made in anesthetized mice and calculated as lead II electrocardiograph by RM6240 multi-channel physiological signal acquisition and processing system (Chengdu, China). The types of alterations (ST-segment elevation or depression) in experimental mice were recorded.

2.15. Echocardiographic assessment of cardiac function

Cardiac structure and function were assessed 24 h post-MI/R injury by a MS-250, 16.0–21.0 MHZ imaging transducer connected to an ultrasonic echocardiographic system (FUJIFILM VisualSonics Vevo 2100, Inc., Toronto, Ontario, Canada.). Under anesthesia, the chest of mice was shaved, and two-dimensional long axis images were captured for end-diastolic and end-systolic volume measurements. The left ventricular ejection fraction (EF, %) and fractional shortening (FS, %) were automatically calculated and recorded by the echocardiographic system. Each parameter was evaluated by calculating the average of five cardiac cycles.

2.16. Blood sample and tissue processing

At the indicated time points, mice were killed by overdose anesthesia with pentobarbital sodium (150 mg/kg, i.p.) and the blood and heart samples were extracted for further analyses.

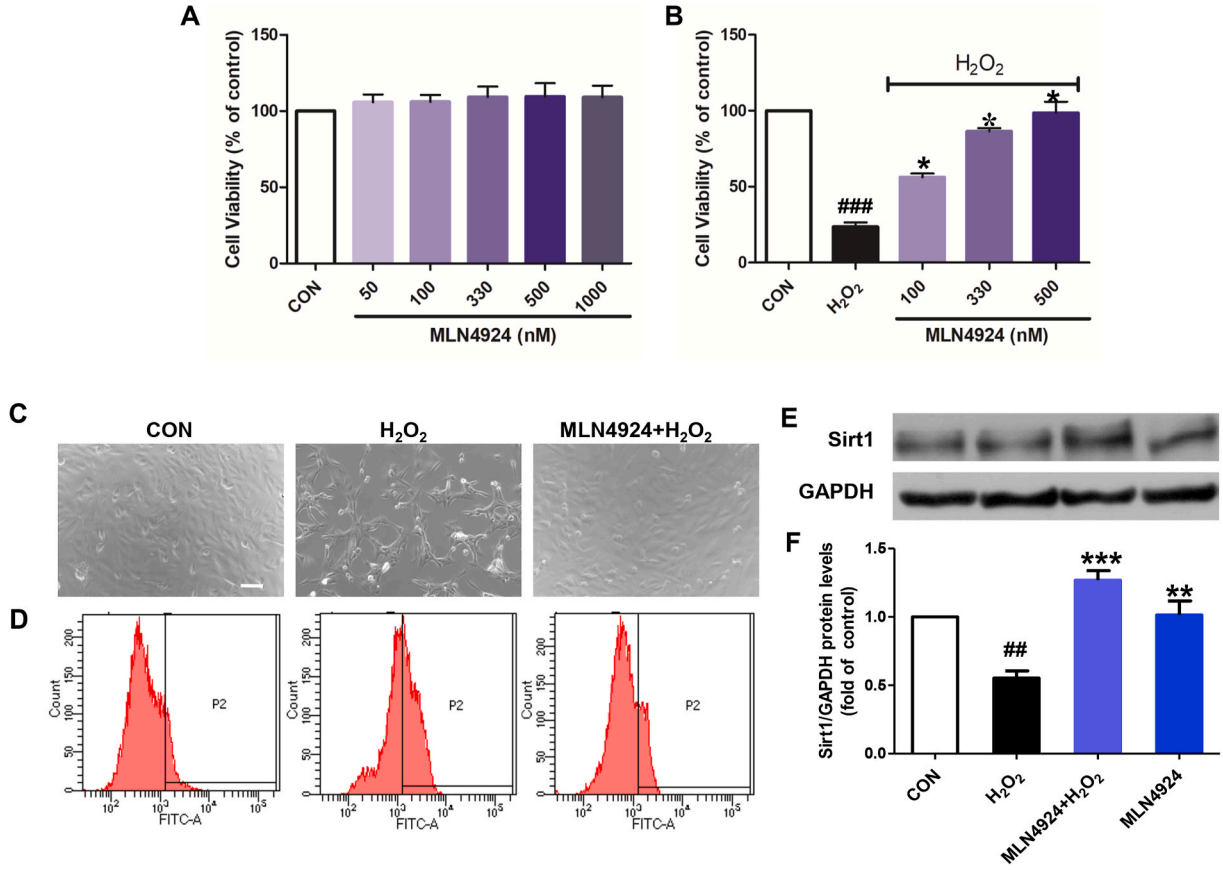

Fig. 1. Effects of MLN4924 on cardiomyocyte death were associated with Sirt1. Cardiomyocytes were treated with (A) MLN4924 only (0.05–1 μM) for 24 h, or (B) MLN4924 (0.1–0.5 μM) followed by H_2O_2 (250 μM) for 2 h. Cell viability was measured using MTS assay. (C) Cell morphology was observed (× 200, bar = 100 μm) and intracellular reactive oxygen species (ROS) generation was measured using the DHE assay. (E–F) Protein level of Sirt1 in cells subjected to H_2O_2 injury was detected. For calculation of relative changes in protein expression, values of individual samples were divided by the mean value of samples from the control group. Microscopic images are representative of three independent experiments. Data were presented as mean ± S.D. (n = 5). Con: control; H_2O_2: simulated H_2O_2-treated only. $^{\#}P < 0.05$ vs. Con; $^{*}P < 0.05$ vs. H_2O_2.

2.17. Detecting of myocardium infarct size

Measurements of area at risk and infarct size were performed as described previously [14]. Briefly, hearts were perfused with 1% Evans' blue dye (Sigma-Aldrich, St. Louis, MO) to delineate the ischemic area at risk (AAR), and then were quickly frozen at −20 °C for 30 min. Thereafter, hearts were sectioned transversely from the apex into 2 mm thick sections. All sections were incubated in 1% 2,3,5-triphenyltetrazolium chloride (TTC, Sigma Co., St Louis, Mo) buffer (pH 7.4) at 37 °C in the dark to determine the unstained necrotic region within the ischemic risk zone. The area at risk and the infarct zone was demarcated and analyzed by Image J software. Risk area% was measured as the ratio of risk area to myocardium × 100. Infarct size was expressed as a percentage of AAR.

2.18. Detecting myocardial enzymes

Activities of CK-MB, LDH, and AST in serum were assayed using commercial kits purchased from Jiancheng Institute of Biotechnology (Nanjing, China).

2.19. Histopathological analysis of heart

Heart tissues were fixed in 10% buffered formalin and embedded in paraffin. For the histological assessment, paraffin embedded tissue sections of heart (4 μm) were stained with hematoxylin-eosin (H&E), and examined microscopically (× 200).

2.20. TUNEL staining of heart section

Apoptosis was analyzed using TUNEL assay (the TUNEL Apoptosis Detection Kit, C1089, Beyotime, Shanghai, China). Apoptotic nucleuses were visualized with light microscopy or fluorescent microscopy. The experiment was repeated on five different sections for each specimen. Ten random fields (× 400) per section were analyzed. Then the average percentage of apoptotic cell was calculated.

2.21. Transmission electron microscopy

Small fragments of myocardium sized ~1 mm^3 were fixed overnight by immersing in 2.5% (w/v) glutaraldehyde, 0.01% picric acid, 0.1 M cacodylate buffer, pH 7.4. After rinsing in the same buffer, the tissues were immersed in 1% (v/v) osmium tetroxide in 0.1 M cacodylate buffer for 1 h followed by block incubation with 2% (v/v) aqueous uranyl acetate for 2 h. Following dehydration in a series of acetone washes, tissues were embedded in Araldite for coronal sections. Ultrathin sections (75–80 nm) at least three blocks per sample were cut with ultramicrotome, collected on 200-mesh copper grids and contrasted with in 5% uranyl acetate in ethanol (10 min) and lead citrate (5 min). Thereafter, grids were examined by transmission electron microscopy (H-7100, Hitachi, Hitachinaka, Japan).

2.22. Western blotting assay

Western blot was performed as described in our previous studies [14,

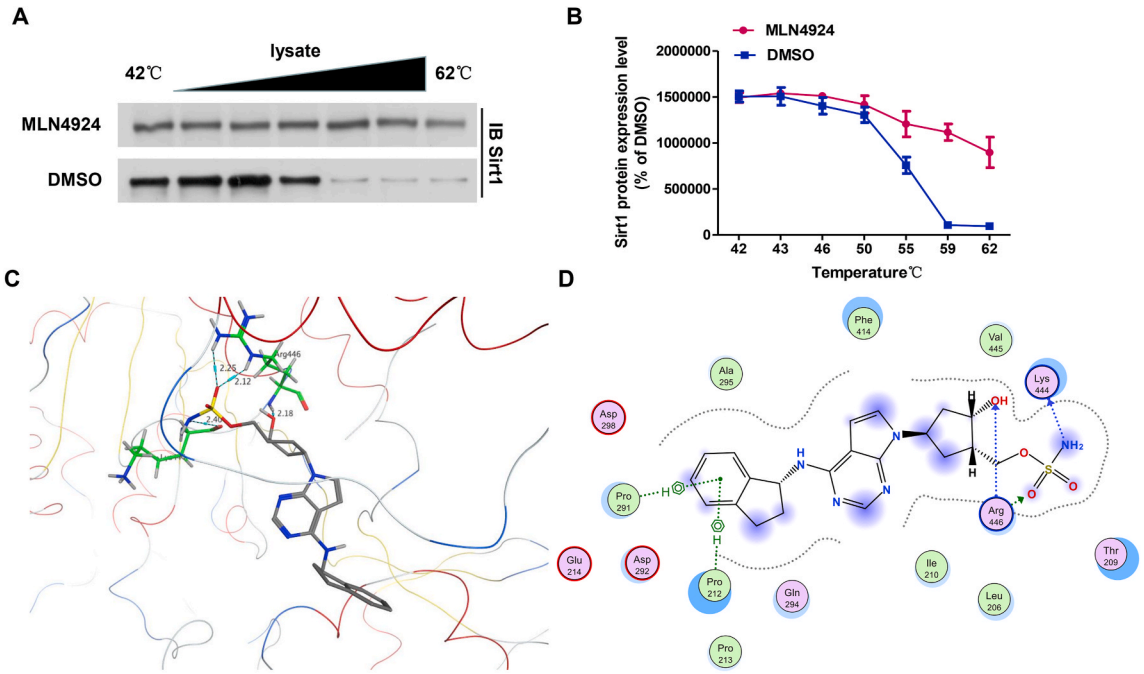

Fig. 2. MLN4924 could interact with Sirt1 protein. (A and B) Cellular thermal shift assay (CETSA) was used to determine the effect of MLN4924 on Sirt1 protein stability. Cardiomyocytes lysates were exposed to MLN4924 (20 μM). (C and D) MLN4924 was docked to the binding pocket of Sirt1.

15]. For cellular samples, cell lysates were obtained using commercial RIPA lysis buffer (Beyotime, China). For heart samples, they were homogenized with commercial RIPA lysis buffer (Beyotime, China). The protein content was determined by using the BCA kit (Beyotime, China). Equal amounts 50 μg/lane of protein were subjected to SDS-PAGE and transferred to PVDF membranes (Millipore Corporation, MA, USA). Blots were blocked for 2 h in 5% nonfat dry milk-TBS-0.1% Tween 20 and then washed. Primary antibodies were incubated overnight at 4 °C followed by a horseradish peroxidase-conjugated secondary anti-rabbit or mouse antibody (1:10,000; Cell Signaling Technology Co., Ltd, MN, USA) for 2 h. Immunoreactivity was detected by the Enhanced Chemiluminescence DetectionReagentssuper Signal West pico Chemiluminescent reagent (34,079, Pierce, Thermo Scientific, Rockford, IL, USA) by a gel imaging system (Protein Simple, Santa Clara, California, USA). The primary antibodies used were polyclonal antibodies against Cul 2 from Abcam (Cambridge, USA); Nrf2, Cul1, 4A, 4B, 5 from Proteintech (1:1000, Proteintech Biotech, Wuhan, China); P62, Atg 5, Beclin-1, LC3I/II, Cul3, HO-1, NQO1 and Sirt1 from Cell Signaling (MN, USA). Protein expression levels were normalized against levels of GAPDH, which was used as a loading control. For calculation of relative changes in protein expression, values of individual samples were divided by the mean value of samples from the control, Ad.GFP control or sham group.

2.23. Statistical analysis

The results are expressed as mean ± SD. One-way ANOVA followed by Tukey's post hoc test or nonparametric Kruskal-Wallis test followed by the Bonferroni test (from GraphPad Prizm 5.0) were used for multigroup comparison. *P* values less than 0.05 were considered significant.

3. Results

3.1. Effects of MLN4924 on cardiomyocyte death through autophagic flux induction and Sirt1 activation

Cell viability and lactate dehydrogenase (LDH) leakage assays were used to assess the effect of MLN4924 on cell viability in H_2O_2-treated H9c2 cells. We found that MLN4924 at up to 100 μM did not show any significant cytotoxicity in H9c2 (Fig. 1A). Thus, lower than 0.5 μM MLN4924 and 250 μM H_2O_2 were chosen in subsequent experiments. Therefore, the intermediate concentration (330 nM) was selected for this subject for follow-up experiments (Fig. 1B). In addition, compared with the control group, morphology of H9c2 cells showed shrinkage and death due to H_2O_2 treatment. Notably, MLN4924 markedly reversed H_2O_2-induced abnormalities (Fig. 1C). The degree of cell damage was monitored by measuring the content of ROS in cardiomyocytes. Results showed that treatment with H_2O_2 induced markedly elevated ROS levels, but pretreatment with MLN4924 (330 nM) markedly reduced ROS level (Fig. 1D).

Meanwhile, to dig into the mechanism of MLN4924, we then investigated the effect of MLN4924 on the expression of Sirt1 proteins against H_2O_2-induced injury in H9c2. We found that H9c2 cells exposed to 250 μM H_2O_2 for 2 h showed markedly decreased level of Sirt1 by 44.7%, compared to the control group (Fig. 1E and F). In addition, MLN4924 group showed markedly increased expression of Sirt1 compared to the H_2O_2 injured cells. Interestingly, administration with MLN4924 significantly up-regulated the expression of Sirt1 by 2.6-fold, compared to the H_2O_2 group. These findings indicate that Sirt1 may be associated with the cardioprotective effect of MLN4924 in H_2O_2-induced cell injury.

3.2. MLN4924 could bind to Sirt1

Next, we explored the interaction between MLN4924 and Sirt1 by CETSA assay. As shown in Fig. 2A and B, Sirt1 was relatively stable between 42 °C and 62 °C in MLN4924 treated cells. However, Sirt1 degraded at 59 °C in DMSO-treated cells. These results indicate that MLN4924 could indeed bind to the Sirt1 protein and increase its thermal stability in cardiomyocytes.

The crystal structure of Sirt1 complexing with its classic resveratrol (PDB ID = 5BTR) was obtained from the RCSB Protein Data Bank (http://www.pdb.org). The protein Sirt1 was prepared with residue correction and hydrogen adding with Amber10: EHT force field. The ligand compound MLN4924 was prepared after optimizing with unrestricted B3LYP [24–26] functional with 6–31G (d, p) basis set using Gaussian16 programs. After docking, 30 poses of the ligand were written and examined, followed by the interaction analyses between the binding

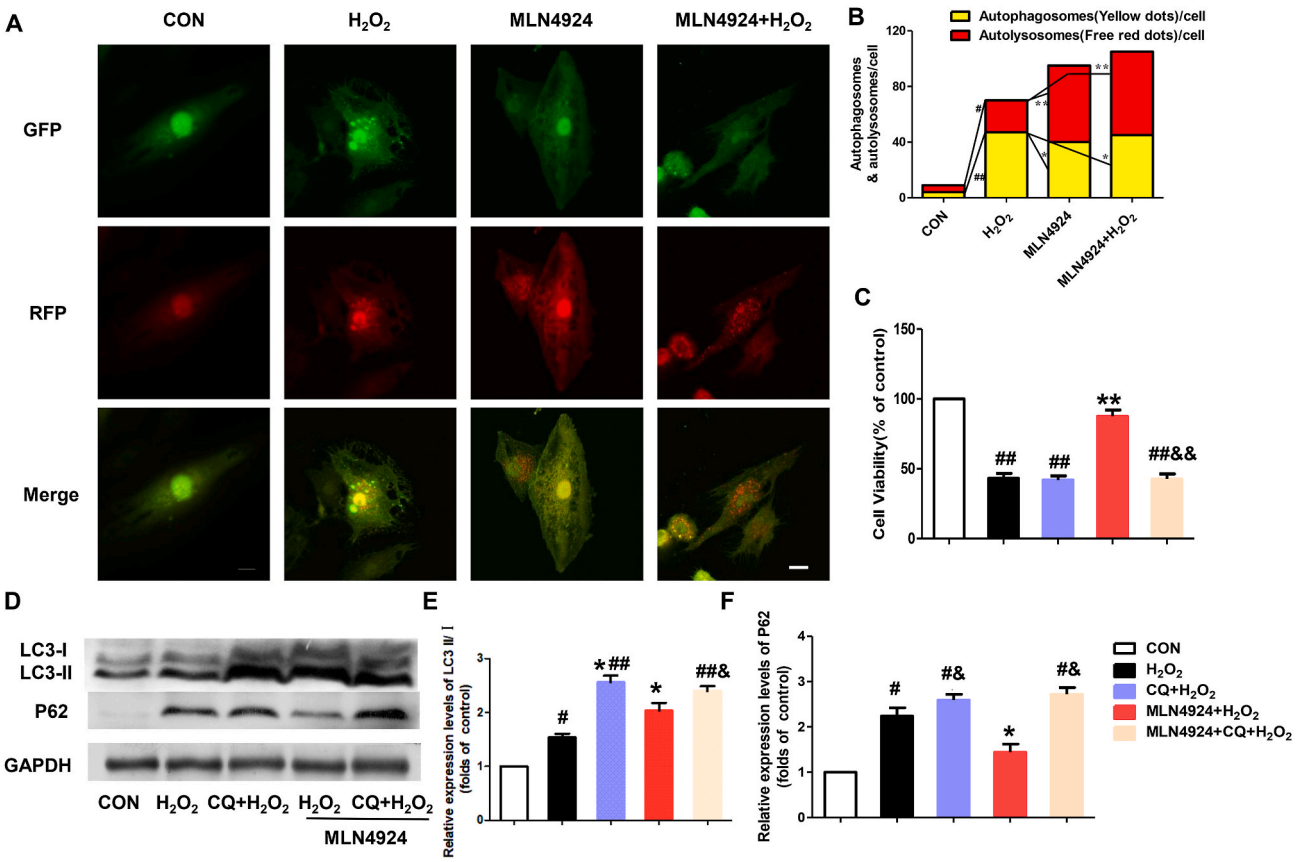

Fig. 3. Effects of MLN4924 on autophagic flux and Nrf2 was Sirt1 dependent. (A) Cardiomyocytes were transfected with adenovirus harboring tandem fluorescent mRFP-GFP-LC3 (Ad-LC3-NRCs) for 24 h. Ad-LC3-NRCs subjected to H_2O_2 were treated with or without 0.33 μM MLN4924. Representative immunofluorescent images of cardiomyocytes expressing mRFP-GFP-LC3 were shown. GFP dots are green. mRFP dots are red. (B) Mean number of autophagosomes (puncta with both red and green colors, ie, puncta with yellow color in merged images) and autolysosomes (puncta with only red but not green color, ie, puncta with red color in merged images) per cell. (C) With or without CQ co-treatment, cell viability was assessed using MTT assays, and (D) Immunoblot analyses were performed. (E–F) Densitometric analyses. For calculation of relative changes in protein expression, values of individual samples were divided by the mean value of samples from the control group. Data were presented as mean ± S.D. (n = 5). Con: control; H_2O_2: simulated H_2O_2-treated only. $^{\#}P < 0.05$ vs. Con; $^{*}P < 0.05$ vs. H_2O_2; $^{\&}P < 0.05$ vs. MLN4924 + H_2O_2. (For interpretation of the references to color in this figure legend, the reader is referred to the Web version of this article.)

pocket of Sirt1 and the top-ranked pose of compound MLN4924 (Fig. 2C and D). These computer-based calculations and findings further confirmed the direct interaction between MLN4924 and Sirt1.

3.3. MLN4924 enhanced autophagic flux in H9c2 exposed to H_2O_2

To further monitor the autophagic flux, tandem fluorescent mRFP-GFP-LC3 was transfected into H9c2 cells (Ad-LC3-H9c2). The control Ad-LC3-H9c2 showed basal autophagy with few autolysosomes and autophagosomes. However, Ad-LC3-H9c2 subjected to H_2O_2 had accumulated autophagosomes and few autolysosomes, suggesting that autophagosome clearance was inhibited and autophagic flux was blocked or impaired in cardiomyocytes during oxidative stress. In MLN4924-treated Ad-LC3-H9c2 cells, subjected to H_2O_2 had more autolysosomes and fewer autophagosomes than those in untreated group (Fig. 3A–B), indicating that MLN4924 treatment could induce the consumption of autophagosomes and further enhanced the autophagic flux in cardiomyocytes.

Chloroquine (CQ), the autophagosome-lysosome binding inhibitor, was added to cardiomyocytes to explore the role of ameliorating the autophagic flux blockage in the cardioprotective effect of MLN4924. CQ (20 μM) treatment further reduced the cell viability caused by H_2O_2, compared to the H_2O_2 alone treated cells. Pretreatment with MLN4924 alone for 24 h significantly increased the cell viability in H9c2 cells subjected to H_2O_2 injury (Fig. 3C). Our data showed that the cell viability had no significant difference between H_2O_2 groups in the presence and absence of CQ. Whereas, CQ (20 μM) significantly reversed the effect of MLN4924 on the cell viability in H9c2 subjected to H_2O_2 injury. To further confirm the role of MLN4924 in the modulation of autophagic flux, we measured the expression levels of autophagy-related proteins. Additionally, Western blot analysis of autophagy proteins (Fig. 3D–F) showed that the ratio of LC3 II/I has been markedly upregulated by H_2O_2+CQ co-treatment relative to that in the H_2O_2 only group, while the level of P62 had no significant differences between these two groups. In contrast, when coadministered with CQ, MLN4924 significantly reduced the accumulation of LC3 II and P62 in H9c2 exposed to H_2O_2, demonstrating that MLN4924 promoted the consumption of autolysosomes. However, CQ abolished the beneficial effect of MLN4924 on the cell viability in H_2O_2-treated H9c2 cells. H_2O_2-induced injury thus increased autophagy and impaired autophagic flux compared with control cells, and MLN4924 exerted a cardioprotective effect that depended on enhancing the cellular autophagic flux.

3.4. Knockdown of Sirt1 blocked the protective effect of MLN4924 on H_2O_2 injury in H9c2

To determine the role of Sirt1 in the beneficial effects of MLN4924 in H9c2 cells, H9c2 cells were infected with Ad.GFP or Ad.Sirt1-AS for 48 h (Fig. 4A), and the levels of Sirt1 were examined (Fig. 4B). In the cells infected with Ad.Sirt1-AS, the level of Sirt1 was decreased by 76.1%, compared to the Ad.GFP control group (Fig. 4B and C). However, no apparent morphological alterations or differences in the number of

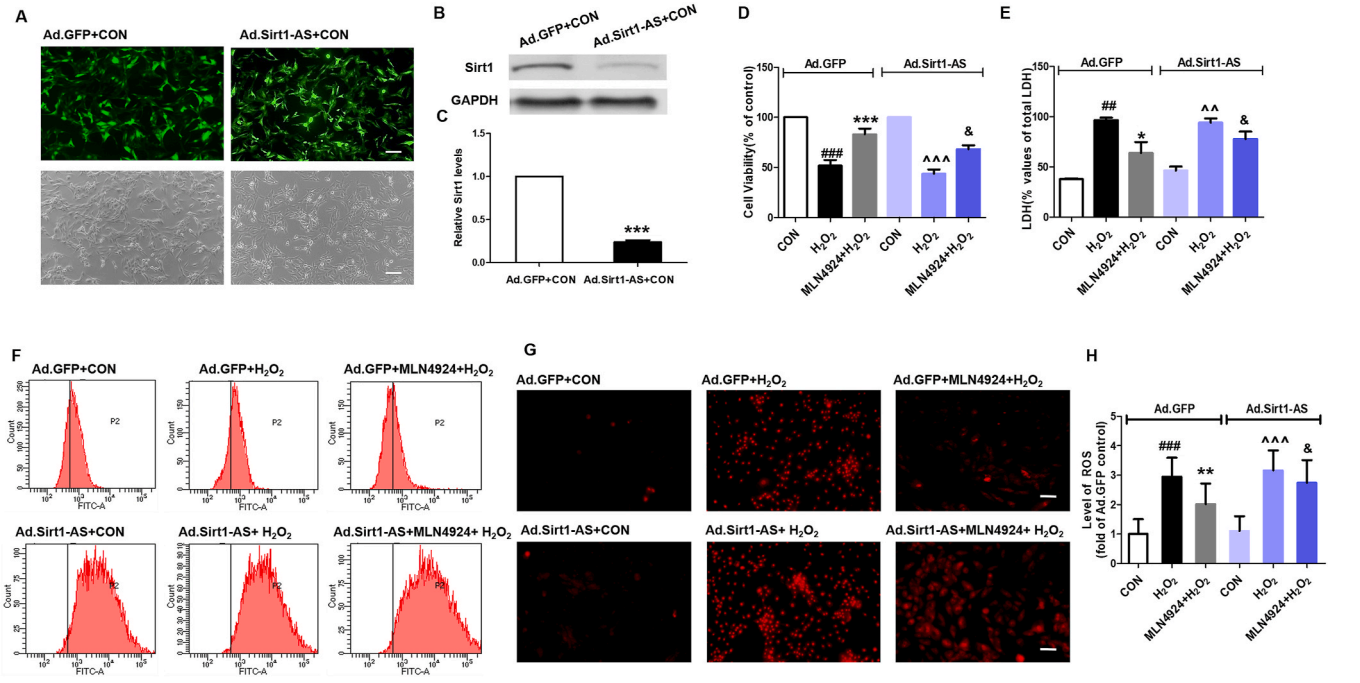

Fig. 4. Knockdown of Sirt1 blocked MLN4924's beneficial effects in H9c2 cardiomyocytes damaged by H_2O_2. Cardiomyocytes were infected with adenoviruses: Ad.GFP or Ad.Sirt1-AS (antisense), under light (× 100, down panel) and fluorescence (× 100, up panel) microscope (bar = 20 μm) (A). Quantitative immunoblotting of Sirt1 was shown (B and C). Cell viability (D), LDH release rate (E) were demonstrated with bar diagram, respectively. Intracellular reactive oxygen species (ROS) generation were assessed with DHE assays (200 × , bar = 400 μm) (F and G). (H) depicts quantitative analysis of the results of intracellular ROS. Data are means ± S.D (n = 5). $^{\#}P < 0.05$ vs. Ad.GFP + CON (control cells infected by Ad.GFP). $^{*}P < 0.05$ vs. Ad.GFP + H_2O_2 (Ad.GFP infected cells treated with H_2O_2). $\hat{}P < 0.05$ vs. Ad. Sirt1-AS + CON (control cells infected by Ad. Sirt1-AS). $^{\&}P < 0.05$ vs. Ad.GFP + H_2O_2+MLN4924.

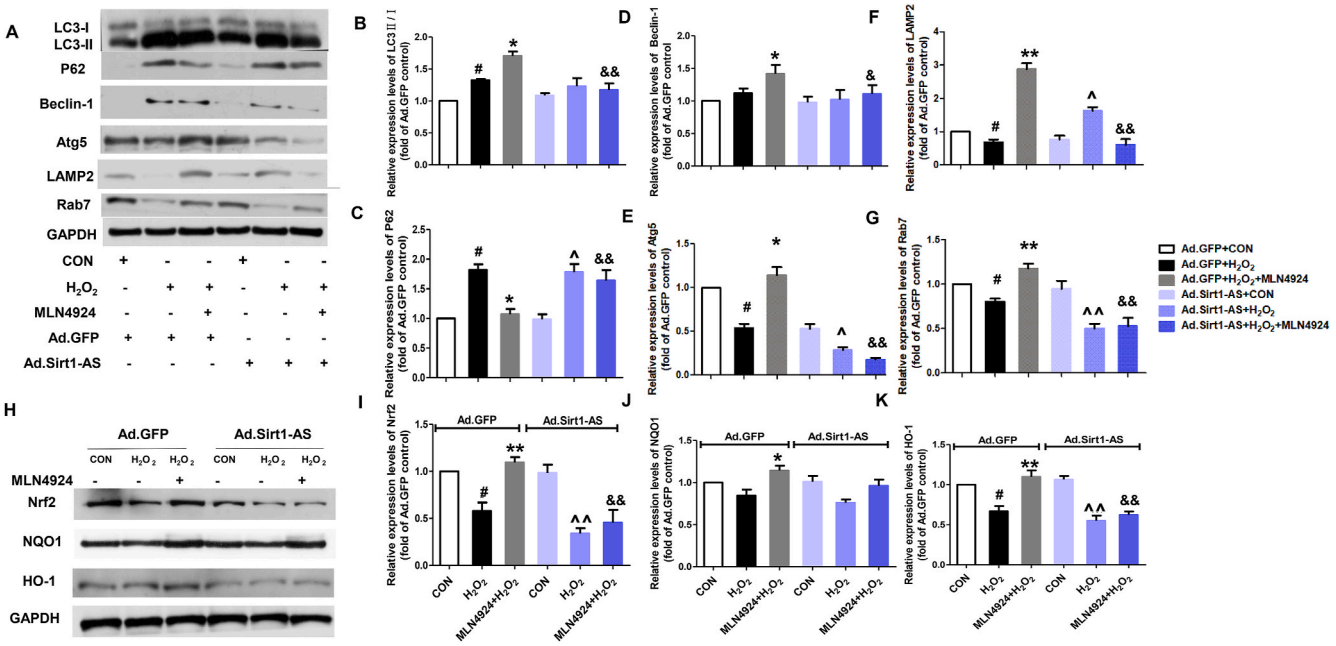

Fig. 5. Effects of MLN4924 on autophagic flux marker proteins. Protein levels of apoptosis-related proteins (LC3II/I, P62, Beclin-1, Atg5, LAMP2, Rab7) were also detected (I–O), and (P–S) protein expressions of Nrf2, NQO1 and HO-1 were determined by Western blot analysis. Protein expression levels were normalized against levels of GAPDH, which was used as a loading control. For calculation of relative changes in protein expression or ROS level, values of individual samples were divided by the mean value of samples from the Ad.GFP control group. Data are means ± S.D (n = 5). $^{\#}P < 0.05$vs. Ad.GFP + CON (control cells infected by Ad.GFP). $^{*}P < 0.05$vs. Ad.GFP + H_2O_2 (Ad.GFP infected cells treated with H_2O_2). $\hat{}P < 0.05$vs. Ad.Sirt1-AS + CON (control cells infected by Ad. Sirt1-AS). $^{\&}P < 0.05$ vs. Ad.GFP + H_2O_2+MLN4924.

adherent cells were observed among the two groups (Fig. 4A).

To identify the role of Sirt1 in the beneficial effects of MLN4924 in H9c2 cells, the infected cardiomyocytes were treated with H_2O_2, and cell viability and the release rate of LDH were examined. Upon H_2O_2 treatment, the cell survival rate of Ad.GFP and Ad.Sirt1-AS groups were reduced to 43.2%, 42%, compared to the Ad.GFP + CON group,

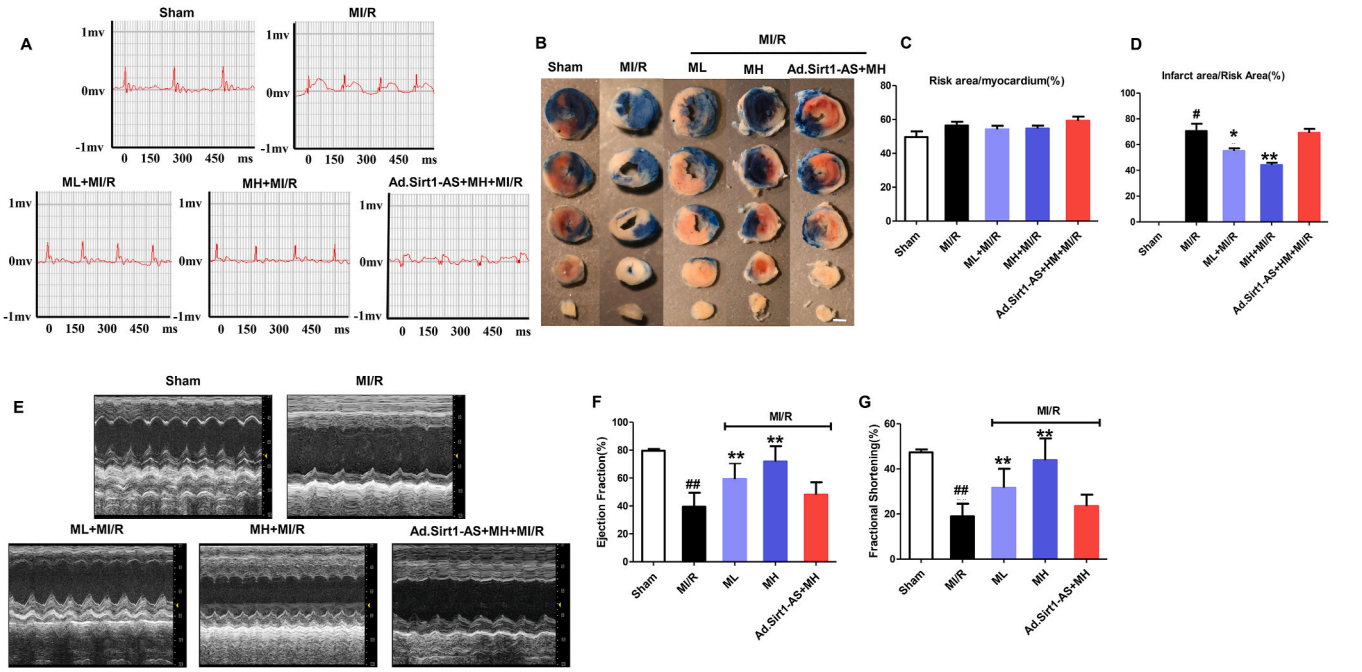

Fig. 6. ECG alterations and cardiac functions melioration induced by MLN4924 in MI/R mice were associated with Sirt1. After intramyocardial Ad. Sirt1-AS delivery for 3 days, all mice were Sham, MI/R, ML (3 mg/kg) +MI/R, MH (6 mg/kg) +MI/R, Ad.Sirt1-AS + MH(6 mg/kg)+MI/R operated. (A) Electrocardiogram (ECG) traces (50 ms/div) was performed 24 h after MI/R injury in mice. Myocardial infarct size (I, bar = 10 mm) (B), ratio of risk area to myocardium (C) and infarct area to risk area (D) in each group were also detected. Additionally, MI/R mice showed a dramatic left ventricular functional impairment as indicated by 2-dimensional M-mode tracing of wall motion, compared with Sham operated animals (E). MLN4924 treatment significantly improved cardiac functions. EF, ejection fraction (F). FS, fractional shortening (G). Data were presented as mean ± S.D.(n = 5). $^{\#}P < 0.05$ vs. Sham group. $^{*}P < 0.05$ vs. MI/R group.

respectively (Fig. 4D).The LDH release rate in Ad.Sirt1-AS + H_2O_2 cells was significantly increased by 77.7%, which was even higher than that in the Ad.GFP + H_2O_2 group (Fig. 4E). Pretreatment with MLN4924 alone significantly restored those abnormalities caused by H_2O_2 in H9c2 cells infected with Ad.GFP. Whereas, cardioprotective action of MLN4924 was significantly blocked in Ad.Sirt1-AS infected cells. These findings indicate that Sirt1 indeed played a key role in the beneficial effect of MLN4924 against H_2O_2-induced injury in H9c2. Thereafter, ROS levels were also measured using a fluorescent probe——DHE. H_2O_2 treatment induced dramatical ROS accumulation in H9c2 cells, as compared to control group (Fig. 4F and G). MLN4924 significantly reduced the ROS accumulation (Fig. 4H). Whereas, down-regulation of Sirt1 almost completely eliminated the myocardial protective of MLN4924.

3.5. *Effects of MLN4924 on autophagic flux and Nrf2 was Sirt1 dependent*

Furthermore, the non-infected or infected cardiomyocytes were treated with H_2O_2, and expressions of autophagic flux related proteins was examined (Fig. 5A). Among non-infected cell groups, H_2O_2 significantly suppressed the protein expressions of Atg5 to 39.2%, LAMP2 to 34.3%, and Rab7 to 19.3% and increased the expression of LC3II/I (~1.3 fold), Beclin1 (~1.1 fold), and P62 (~1.8 fold) in H_2O_2 groups (Fig. 5A–G). Whereas, pretreatment with MLN4924 significantly increased the expressions of LC3II/I (~1.3 fold), Beclin1 (~1.3 fold), Atg5 (~1.9 fold), LAMP2 (~3 fold), and Rab7 (~1.5 fold) in H9c2 cells exposed to H_2O_2. Pretreatment also reduced P62 protein level compared with its level in Ad.GFP + H_2O_2 (Fig. 5A–G), indicating that MLN4924 promoted the degradation of autolysosomes. Thus, autophagosome accumulation may be caused by H_2O_2-induced impaired autophagy. However, MLN4924 pretreatment could induce a significant clearance of autophagosomes with the degradation of autolysosome. While, down-regulation of Sirt1 profoundly increased the expressions of P62 and decreased that of Atg5 and Rab7. Importantly and notably, knock down of Sirt1 amazingly diminished the effect of MLN4924 on ameliorating the autophagic flux blockage in the presence of H_2O_2, demonstrated by markedly reduced expressions of Atg5 and Rab7, as well as the up-regulation of P62.

Additionally, we also detected the alterations of Nrf2, as well as HO-1 and NQO1 among experimental groups (Fig. 5H). MLN4924 significantly up-regulated the expressions of Nrf2 (~1.9–fold), HO-1 (~1.3–fold), and NQO1 (~1.6–fold), respectively, compared to those in Ad.GFP + CON group (Fig. 5H–K). Upon H_2O_2 treatment, over-expression of Sirt1 further increased the levels of Nrf2, HO-1 and NQO1 relative to those in Ad.GFP + H_2O_2 group. Notably, down-regulation of Sirt1 markedly diminished the effects of MLN4924 on induction of these endogenous antioxidative enzymes in the presence or absence of H_2O_2 (Fig. 5H–K). These findings suggested that Sirt1 indeed played a key role in mediating MLN4924's effect on autophagic flux impairment.

3.6. *MLN4924 ameliorated MI/R injury via Sirt1 in vivo*

To further confirm the involvement of Sirt1 in MLN4924's cardioprotection *in vivo*, the following experiment was performed accordingly by intramyocardial injection of Ad.Sirt1-AS. We found that compared to the sham group, dramatic ST segment elevation by ECG at 24 h reperfusion was observed in MI/R group (Fig. 6A), while ML (3 mg/kg) and MH (6 mg/kg) reduced ST segment elevation to varying degrees. However, downregulation of Sir1 by Ad.Sirt1-AS significantly reversed the effect of MLN4924 on the ST segment elevation. Furthermore, an apparent increase in myocardial infarction was observed in MI/R group (70.6%). ML (3 mg/kg) and MH (6 mg/kg) significantly reduced the infarct size to 55%, 44.1%, compared to the MI/R group (Fig. 6B–D). However, downregulation of Sirt1 significantly reversed the infarct size (69.2%) to the level of MI/R group (Fig. 6B).

Furthermore, at 24 h post-MI/R, compromised heart function was

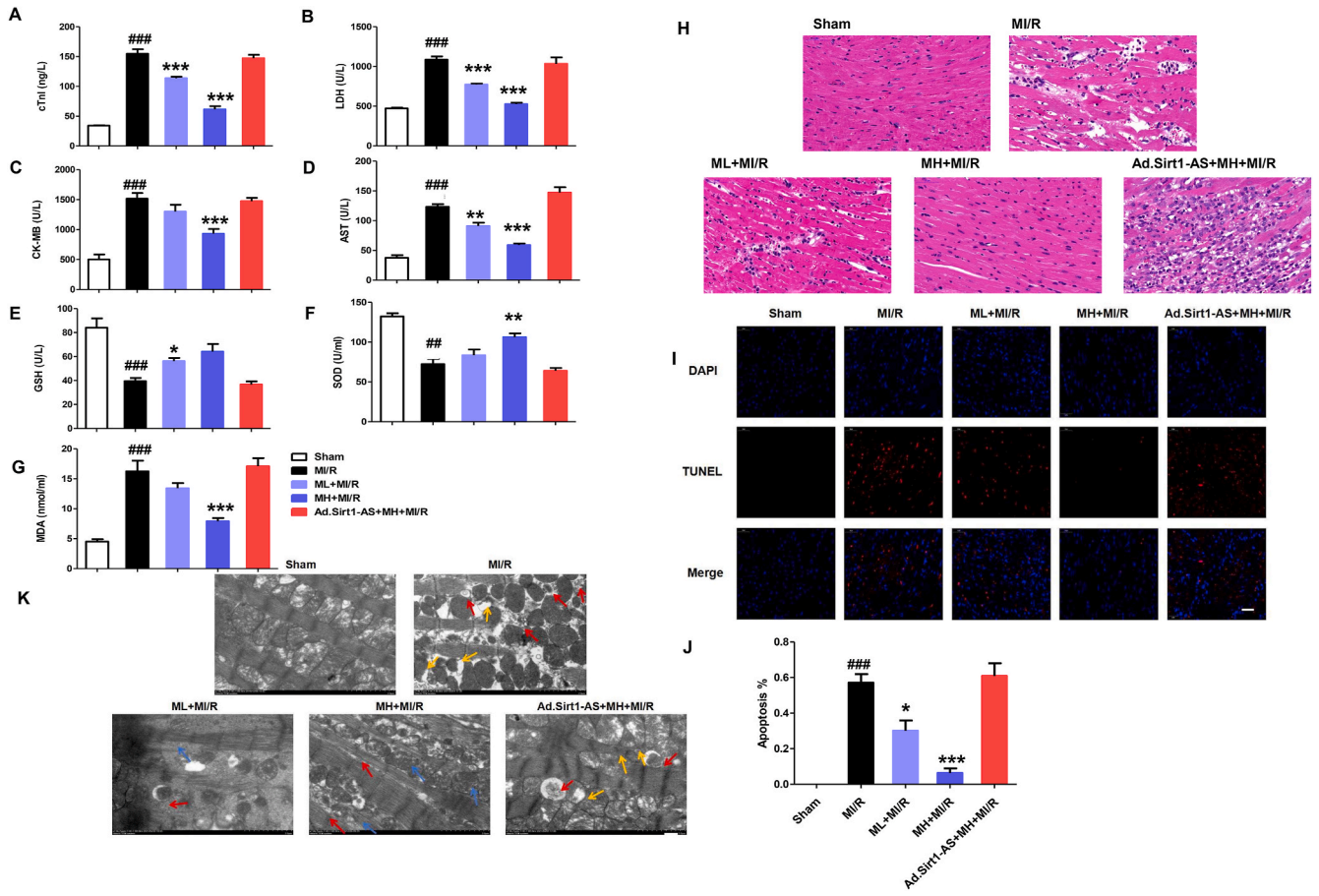

Fig. 7. Biochemical alterations and anti-apoptosis effect of MLN4924 in MI/R mice was associated with Sirt1. Levels of serum marker enzymes cardiac troponin I (cTnI) (A), lactate dehydrogenase (LDH) (B) and creatine kinase-MB (CK-MB) (C) were detected in all experimental groups, respectively. Content of aspartate transaminase (AST) (D), MDA (G) and levels of endogenous anti-oxidant enzyme system including glutathione (GSH) (E), superoxide dismutase (SOD)(F) in serum were also analyzed. Additionally, (H) exhibits the representative H&E images of heart tissue (× 200, bar = 50 μm). In addition, representative photomicrographs of terminal deoxynucleotidyl transferase mediated dUTP nick end labeling (TUNEL) staining in myocardial layers within the ischemic/reperfused area at risk were also examined (400 × , bar = 200 μm, I and J). (R) Myocardial ultrastructure was observed light microscopy and transmission electron microscope (× 7000, bar = 4 μm, K), respectively. Data were presented as mean ± S.D. (n = 5). $^{\#}P < 0.05$ vs. Sham group. $^{*}P < 0.05$ vs. MI/R group.

observed in the MI/R animals, as (Fig. 6E) demonstrated by significant decreases in EF% (39.4%, Fig. 6F) and FS% (18.9%, Fig. 6G), respectively, compared with the sham group. However, treatment with ML and MH depicted significant improvement in EF% and FS%: 59.3% and 71.8%, and 31.7% and 42.2%, respectively. Notably, down-regulation of Sirt1 significantly impaired the protective effects of MLN4924 on EF% and FS%. As for alterations of myocardial zymogram in serum, a marked elevation in the activities of cTnI, CK-MB and LDH were observed in MI/R mice. ML and MH group significantly reduced these activities of cTnI, CK-MB and LDH of those in MI/R mice, respectively (Fig. 7A–D). However, down-regulation of Sirt1 significantly reversed the beneficial effects of MLN4924 on the myocardial zymogram levels (Fig. 7A–D). Meanwhile, the significantly increased content of MDA, markedly declined level of GSH and activity of SOD were observed in MI/R and Ad.GFP + MI/R group, respectively, compared to those in Sham mice. However, ML (3 mg/kg) and MH (6 mg/kg) prevented the GSH, SOD decrease, the MDA further increase, respectively, relative to those in Ad.GFP + MI/R group (Fig. 7E–G). Accordingly, down-regulation of Sirt1 resulted in further decreased decreases of GSH, SOD, and the MDA increase, compared to the Ad.GFP + MI/R mice (Fig. 7E–G).

3.7. MLN4924 ameliorated MI/R injuried cardiac function via Sirt1 in vivo

We further observed the alterations of histopathological structure of heart tissue and ultrastructure of cardiomyocytes. Hearts from the Sham group exhibited clear integrity of myocardial membrane, neatly arranged muscle fibers, no inflammatory cell infiltration (Fig. 7H). However, both of the MI/R and Ad.Sirt1-AS + MH + MI/R groups were observed serious oedema, massive neutrophil infiltration, nuclear pyknosis, cardiomyocyte lysis and necrosis. Whereas, MLN4924 (3 and 6 mg/kg) treatment markedly reversed such abnormal alterations. Moreover, TUNEL staining was performed to estimate the apoptosis. The number of apoptotic cells significantly increased in mice subjected to MI/R. By contrast, pretreatment with MLN4924 (3 and 6 mg/kg) revealed fewer apoptotic cells, respectively. Notably, in Ad.Sirt1-AS + MH infected mice, this value was significantly enhanced to even higher levels than that in MI/R group (Fig. 7I and J).

Transmission electron microscopy (TEM) is the most important method for detecting autophagy. To determine whether MLN4924 regulated autophagic flux, we investigated autophagosomes and autophagolysosome by TEM (Fig. 7K). The results showed that the myocardial fibrils of Sham group were neatly and regularly arranged, the sarcomere and Z line were clear, and the mitochondria were normal shaped. In MI/R and Ad.Sirt1-AS + MH + MI/R groups, however, the myocardial myofibrils were irregularly arranged, myofilament, broken and dissolved, number of damaged mitochondria were profoundly increased with swelling and rounding, even vacuoles and autophagosomes were obviously accumulated, and the autophagy flow was blocked. In contrast, the muscle fibers of ML group were intertwined, the

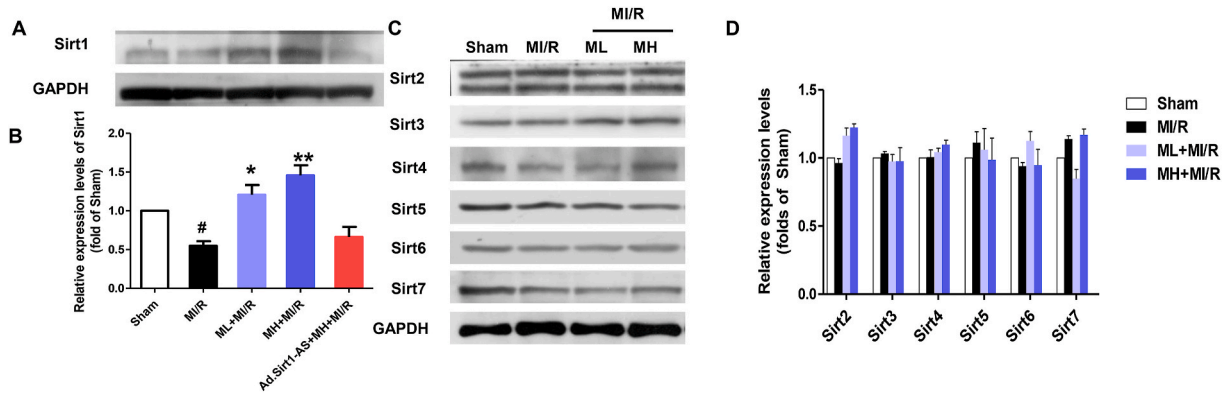

Fig. 8. MLN4924 only up-regulated Sirt1 expression. Quantitative immunoblotting of Sirt1, and the other Sirtuins family expression levels in infected cardiomyocytes were also examined (A–D). Data were presented as mean ± S.D.(n = 5). $^{\#}P < 0.05$ vs Sham group. $^{*}P < 0.05$ vs. MI/R group.

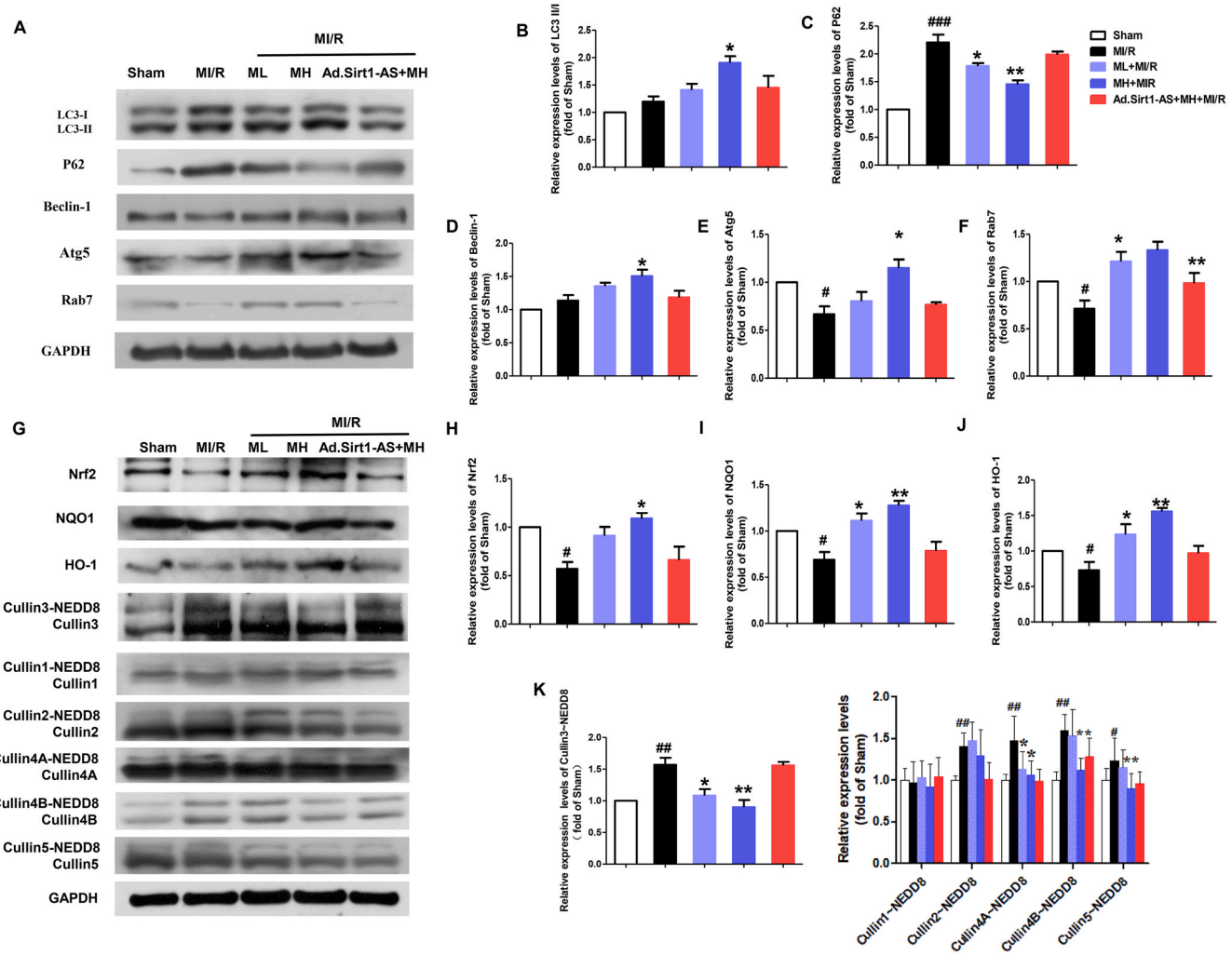

Fig. 9. MLN4924 induced autophagic flux and up-regulated Nrf2 in MI/R mice via Sirt1. Cardiac protein levels of LC3II/I, P62, Beclin-1, Atg5 and Rab7 in Sham and MI/R mice were detected for five independent experiments, respectively (E–K). Effect of MLN4924 on protein levels of Cullin substrate proteins (Nrf2, NQO1, HO-1 and NEDD8 modification of Cullin1, 2, 3, 4A, 4B and 5) (L–P). Data were presented as mean ± S.D. (n = 5). $^{\#}P < 0.05$ vs. Sham group. $^{*}P < 0.05$ vs. MI/R group.

degree of myofilament breakage and dissolution was reduced, the mitochondria were swollen, and autophagosome–lysosome fusion increased; MH group myofibrils had the same line, the mitochondria were basically intact, and the autophagy-lysosome fusion further increased (Fig. 7K). Notably, these data implicated that MLN4924 exhibited a potent cardioprotective effect against MI/R injury by modulating the impaired autophagic flux via Sirt1 *in vivo*.

3.8. MLN4924 induced autophagic flux and up-regulated Nrf2 in mice MI/R via Sirt1

Since the Sirtuins are believed to play an important role in the heart,

changes in expressions of all Sirtuins family members, including 1–7, were checked in myocardial I/R injured hearts (Fig. 8A–D). In the heart of MI/R mice, with or without MLN4924 treatment, none of these proteins was significantly altered, compared to those in Sham (Fig. 8C and D). However, we found that cardiac Sirt1 level was significantly declined by 53.1% in MI/R relative to Sham group. Administration with 3 or 6 mg/kg MLN4924 produced a significant increase in Sirt1 by up to 2.2- and 1.5-fold, respectively, as compared with the Sham group (Fig. 8A and B). Our results strongly indicated that MLN4924 pretreatment only up-regulated the Sirt1 protein expression in the myocardium.

Furthermore, to clarify whether MLN4924 attenuated the blocked autophagic flow in cardiomyocytes by regulating Sirt1, autophagosomes and autophagosome-related proteins were examined (Fig. 9A–F). Quantitative immunoblotting data showed that the expression of LC3II/I, Beclin-1, and P62 in myocardial tissue was significantly up-regulated to ~1.2, ~1.1, and ~2.2-fold, respectively, in the MI/R model group, compared with the Sham group. While the cardiac expressions of Atg5 and Rab7 markedly decreased by 33.3% and 28.9% in MI/R mice, respectively, compared with the Sham group. Compared with the MI/R model group, LC3II/I, Beclin-1, Atg5, Rab7 protein expressions were up-regulated in heart tissues of the ML group to ~1.2, ~1.2, ~1.2, and ~1.7 fold, and P62 protein expression level decreased by 19.2%, respectively. LC3II/I, Atg5, Beclin-1, Rab7 (~1.6, ~1.3, ~1.7, and ~1.9–fold) protein expression was significantly higher in the MH group, respectively, as well as the significantly decreased expression of P62 by 34.1%, compared with those in MI/R model group. However, cardiac expressions of autophagic flux-related proteins in the Ad.Sirt1-AS + MLN4924 group were not significantly altered, relative to those in MI/R mice. Therefore, Sirt1 played an important role in MLN4924' action on improving the blocked autophagic flux in cardiacmyocytes during MI/R.

Levels of NEDD8 modified Cullins family members and protein expressions of Nrf2and its downstream proteins (i.e., HO-1 and NQO1) were also detected to confirm the inhibitory effect of MLN4924 on neddylation (Fig. 9G–K). Our results pictured that MI/R injury was closely associated with significant increases in the Cullin3~NEDD8 (~1.6 fold), along with markedly decreased Nrf2 to 43.1%, HO-1 to 31% and NQO1 to 27%, compared to those in Sham animals. However, ML (3 mg/kg) and MH (6 mg/kg) pretreatment differentially reversed such abnormal alterations and further increased the expression of Nrf2 and its downstream proteins (i.e., HO-1 and NQO1). In contrast, after knockdown the cardiac expression of Sirt1, the levels of Cullin3~NEDD8 modification, as well as Cullin 3 substrate protein Nrf2 and its downstream proteins HO-1 and NQO1, in the heart tissue of MLN4924 pretreatment group was not significantly different from those in MI/R model group. Notably, knockdown of cardiac Sirt1 showed no significant effects on NEDD8 modification of Cullin 1, 2, 4A, 4B and 5 regulated by MLN4924, indicating the important role of Sirt1 in Cullin3~NEDD8 regulated by MLN4924 treatment.

4. Discussion

The NEDD8 conjugation pathway is known as Neddylation. Neddylation regulates a variety of cellular processes, functioning from protein transcription, cell signal transduction to autophagy [27], from neuroprotective action, anti-tumor progression to cardiac chamber development and cardiomyocyte survival [28–32]. However, the potential cardioprotective effect of Neddylation pathway against MI/R injury has not been evaluated. The current results of MTT experiment showed that MLN4924, a selective inhibitor of Neddylation, had no toxic effect on H9c2 cardiomyocytes. MLN4924 (330 nM) pretreatment exerted a strong cardioprotective effect, demonstrated by significantly elevated cell viability, markedly decreased LDH leakage rate, and improved cell morphology in H_2O_2-induced injury *in vitro*. Additionally, MLN4924 (3 and 6 mg/kg) pretreatment in mice markedly improved cardiomyocyte membrane stability, evidenced by decreased levels of serum myocardial zymogram and ameliorated cardiac histopathological alterations, compared to the MI/R mice. Excitingly, we found that MLN4924 not only alleviated the contractile dysfunction of left ventricular, but also declined the abnormally large IS induced by MI/R *in vivo*. Therefore, pre-administration with MLN4924 indeed exerted a strong cardioprotective effect against MI/R injury both *in vitro* and *in vivo*.

Autophagy, induced by oxidative stress and possessing close cross-talk with cell death, apoptosis and endoplasmic reticulum stress, as well as ferroptosis, has been known as a double-edged sword in cardioprotection [33–40]. Recently, scientists have demonstrated the dynamic processes of autophagy, termed the autophagic flux, involving autophagosome formation, fusion of autophagosomes to lysosomes, and degradation in lysosomes, each of which is governed by multiple signaling mechanisms [5]. Importantly, a severe defective autophagic flux would prevent the clearance of damaged intracellular organelles and proteins during myocardial reperfusion after a short period of ischemia because of the accumulation of impaired autophagosome [4,5,41]. In the present study, CQ, the lysosomal inhibitor, was employed as the major tool for evaluating the effects of MLN4924 pretreatment on the autophagic flux *in vitro*. In agreement with the previous investigations [42], CQ dramatically elevated LC3-II/I ratio and P62 level, suggesting the late phase of autophagic flux blocked by CQ, thus aggravating the cardiomyocyte death. Notably, the positive roles of MLN4924 in autophagosome clearance and cell viability were abrogated under a combined treatment with the autophagic flux inhibitor CQ in H_2O_2-stressed cells. These results indicated that the cardioprotective action of MLN4924 depended on its effect on recovering impaired autophagic flux. The autophagic flux monitored by mRFP-GFP-LC3 assay illustrated that MLN4924 restored the defective autophagic flux via enhancing the autolysosome formation *in vitro*.

The class III NAD^+ dependent deacetylases-sirtuins (Sirts) regulate autophagy in many cells in response to cellular stress, including osteosarcoma and mesothelioma cells and cardiomyocytes [43,44]. In the present study, the expression of the members of the sirtuin family of proteins (Sirt1–7) revealed that only Sirt1 was significantly elevated by MLN4924 pretreatment in MI/R mice *in vivo*. Excitingly, Sirt1 has important physiological and pathological significance in cardiovascular diseases, especially for MI/R [45]. Studies have found that Sirt1 can exert cardioprotection by influencing cellular autophagy [46]. Importantly, Sirt1 could promote the starvation-induced autophagic flux blockage in cardiomyocytes [47]. Recently, increased expression of Sirt1 has been demonstrated to elevate autophagic flux in gastric cells, HUVECs, the cortex of cardiac arrest and cardiopulmonary resuscitation mice [48–50]. Moreover, the activation of Sirt1 could enhance the cardiac autophagic flux, thus reducing MI/R-induced oxidative damage, inflammation and apoptosis [51,52]. Furthermore, Cullin-RING E3 ubiquitin ligases (Cullin-RING ligases, CRLs) are, to date, the most thoroughly identified and the largest Neddylation modification ligase E3 in mammals [27,53]. The catalytic activity of CRLs requires the activation of Cullin–NEDD8 [27]. Therefore, the activity of CRLs could be regulated by regulating the NEDD8 modification of Cullins family members. This activity, in turn, affects many physiological and pathological processes [54]. Accumulated reports have demonstrated that CRL3 is closely related to the regulation of autophagy in cells, especially in cardiomyocytes [55]. Meanwhile, MLN4924 has been confirmed to the regulate autophagy, depending on CRL3. Similarly and excitingly, down-regulation of Sirt1 was observed to markedly decrease the levels of Cullin-3–NEDD8 levels but not that of other Cullin family members *in vivo*, along with inhibition of the up-regulated Nrf2 signaling pathway, the specific substrate of Cullin-3–NEDD8, induced by MLN4924 *in vitro* and *in vivo* in the present study. This observation implied that MLN4924 may regulate the cardiac oxidative stress and autophagic flux impairment by modifying the NEDD8 modification of Cullin-3 via Sirt1.

Additionally, the involvement of Sirt1 in the mechanisms underlying the effect of MLN4924 on regulating impaired autophagic flux in MI/R was further investigated by antisense Sirt1 adenovirus interference *in vitro*, and by intramyocardial delivery of it mediated cardiac-specific

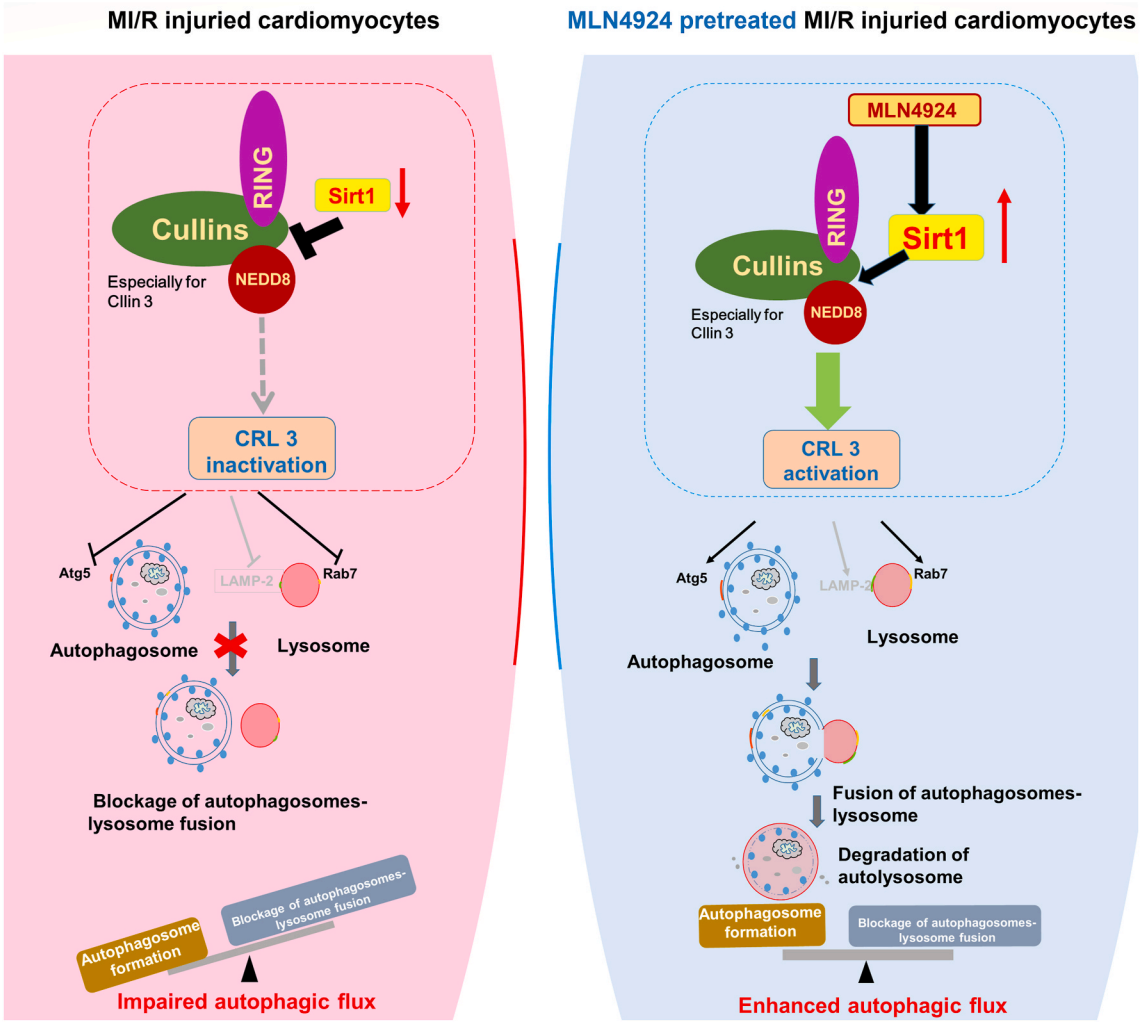

Fig. 10. This program summarizes the potential mechanism of MLN4924 enhancing the autophagic flux in cardiomyocytes against MI/R injury via Sirt1. Left: MI/R injuried myocyte; Right: MLN4924 treated MI/R injuried myocyte.

gene knockdown of Sirt1 *in vivo* 3 days before MI/R, respectively. The increased levels of autophagy substrates P62 implied a decrease in the effective lysosomal degradation [56]. In the present study, the expression levels of the LC3-II were observed significantly increased, whereas that of P62 markedly declined both *in vitro* and *in vivo*. In addition, deficiency in autophagy-related gene (Atg) 5 and lysosomal-associated membrane protein (LAMP) 2 has been demonstrated to exacerbate the MI/R injury via autophagic flux impairment in diabetes [57]. Atg5 also provides novel insights into the interplay between apoptosis and autophagy [58]. Rab7, the autophagosome–lysosome fusion-promoting protein, has been further detected to determine the possible mechanism underlying the enhancement of autophagic flux induced by MLN4924 in the current study. Notably, knockdown of Sirt1 led to remarkable elevation of P62 levels in cardiomyocytes subjected to H_2O_2, indicating a block in the fusion of autophagosomes and lysosomes. Additionally, the profoundly down-regulated levels of Atg5 and Rab7 further supported the deteriorated autophagic flux deficiency caused by Sirt1 knockdown *in vitro*. Excitingly, pretreatment with MLN4924 significantly up-regulated the expressions of Atg5 and Rab7 both in H_2O_2 injured cardiomyocytes and in MI/R mice. As expected, Sirt1 deficiency largely blocked such beneficial effect of MLN4924 *in vitro* and *in vivo*, suggesting that Sirt1 indeed played a pivotal role in promoting autophagosome–lysosome fusion induced by MLN4924. TEM, histopathological assay and TUNEL detection of the heart tissues showed that the absence of Sirt1 blocked the cardioprotective effect of MLN4924 by further exacerbating the impaired autophagic flux in MI/R injury *in vivo*. These observations supported the findings discovered *in vitro*.

5. Conclusions

In summary, to the best of our knowledge, this study is the first to highlight MLN4924 as a critical cardioprotective agent for cardiomyocyte survival in MI/R. Importantly, our work implicated Sirt1 as a crucial factor involved in MLN4924-induced enhancement of cardiac autophagic flux using both *in vitro* and *in vivo* myocardial injury models. Furthermore, we uncovered a novel Sirt1/Rab7 autophagic flux regulation pathway under MI/R stress (Fig. 10).

Author contributions

Bo Wei and Ji Zhang conceived the project. Bo Wei, Ji Zhang and Longhua Yang secured the funding. Bo Wei, Jing Cui, Fei Zhao and Longhua Yang designed and performed the experiments. Xueli Xu and Yangyang Shi analyzed the data. Bo Wei and Ji Zhang provided critical discussion, editing and final approval of the manuscript.

Declaration of competing interest

The authors declare that the research was conducted in the absence of any commercial or financial relationships that could be construed as a

potential conflict of interest.

Acknowledgements

We gratefully acknowledge financial support by the National Natural Science Foundation of China (Grant No. U1904154, 81703598, 21803058), and the Certificate of postdoctoral research grant in Henan province (No. 1902002). We also appreciate the hardware and software support and computer time of Zhengzhou University, Henan Supercomputing Center. We thank Liwen Bianji (Edanz) (www.liwenbianji.cn/) for editing the English text of a draft of this manuscript.

References

[1] M. Zhai, B. Li, W. Duan, J. Lin, S. Yu, Melatonin ameliorates myocardial ischemia reperfusion injury through sirt3-dependent regulation of oxidative stress and apoptosis, J. Pineal Res. 63 (2017).
[2] N. Hariharan, Y. Maejima, J. Nakae, J. Paik, R.A. Depinho, J. Sadoshima, Deacetylation of foxo by Sirt1 plays an essential role in mediating starvation-induced autophagy in cardiac myocytes, Circ. Res. 107 (2010) 1470–1482.
[3] S. Ma, Y. Wang, Y. Chen, F. Cao, The role of the autophagy in myocardial ischemia/reperfusion injury, Biochim. Biophys. Acta 1852 (2015) 271–276.
[4] X. Ma, H. Liu, S.R. Foyil, R.J. Godar, A. Diwan, Autophagy is impaired in cardiac ischemia-reperfusion injury, Autophagy 8 (2012) 1394–1396.
[5] X. Ma, H. Liu, S.R. Foyil, R.J. Godar, C.J. Weinheimer, J.A. Hill, et al., Impaired autophagosome clearance contributes to cardiomyocyte death in ischemia/reperfusion injury, Circulation 125 (2012) 3170–3181.
[6] G. Filomeni, D.D. Zio, F. Cecconi, Oxidative stress and autophagy: the clash between damage and metabolic needs, Cell Death Differ. 22 (2015) 377–388.
[7] Q. Wang, W. Guo, B. Hao, X. Shi, Y. Lu, C.W.M. Wong, et al., Mechanistic study of Trpm2-Ca^{2+}-Camk2-Becn1 signaling in oxidative stress-induced autophagy inhibition, Autophagy 12 (2016) 1340–1354.
[8] T.A. Soucy, P.G. Smith, M.A. Milhollen, A.J. Berger, S.P. Langston, An inhibitor of NEDD8-activating enzyme as a new approach to treat cancer, Nature 458 (2009) 732–736.
[9] A. Andérica-Romero, J. Hernández-Damián, G.I. Vázquez-Cervantes, I. Torres, J. Pedraza-Chaverri, The MLN4924 inhibitor exerts a neuroprotective effect against oxidative stress injury via Nrf2 protein accumulation, Redox Biol 8 (2016) 341–347.
[10] Q. Deng, J. Zhang, Y. Gao, X. She, Y. Wang, Y. Wang, et al., MLN4924 protects against bleomycin-induced pulmonary fibrosis by inhibiting the early inflammatory process, Am J Transl Res 9 (2017) 1810–1821.
[11] Z. Luo, Y. Pan, L.S. Jeong, J. Liu, L. Jia, Inactivation of the Cullin (cul)-RING E3 ligase by the NEDD8-activating enzyme inhibitor MLN4924 triggers protective autophagy in cancer cells, Autophagy 8 (2012) 1677–1679.
[12] T.J. Ai, J.Y. Sun, L.J. Du, C. Shi, C. Li, X.N. Sun, et al., Inhibition of neddylation by MLN4924 improves neointimal hyperplasia and promotes apoptosis of vascular smooth muscle cells through P53 and P62, Cell Death Differ. 25 (2018) 319–329.
[13] C.A. Reihe, N. Pekas, P. Wu, X. Wang, Systemic inhibition of neddylation by 3-day MLN4924 treatment regime does not impair autophagic flux in mouse hearts and brains, Am J Cardiovasc Dis 7 (2017) 134–150.
[14] B. Wei, Q. Lin, Y.-G. Ji, Y.-C. Zhao, L.-N. Ding, W.-J. Zhou, et al., Luteolin ameliorates rat myocardial ischaemia-reperfusion injury through activation of peroxiredoxin II, Br. J. Pharmacol. 175 (2018) 3315–3332.
[15] L. Qiao, C. Xiu-Ying, Z. Ji, Y. Yong-Liang, Z. Wen, W. Bo, Upregulation of Sirt1 contributes to the cardioprotective effect of rutin against myocardial ischemia-reperfusion injury in rats, J Funct Foods 46 (2018) 227–236.
[16] C. Kilkenny, W. Browne, I.C. Cuthill, M. Emerson, D.G. Altman, Animal research: reporting *in vivo* experiments: the arrive guidelines, Br. J. Pharmacol. 160 (2010) 1577–1579.
[17] J.C. McGrath, G.B. Drummond, E.M. McLachlan, C. Kilkenny, C.L. Wainwright, Guidelines for reporting experiments involving animals: the arrive guidelines, Br. J. Pharmacol. 160 (2010) 1573–1576.
[18] R. Serpi, A.M. Tolonen, J. Huusko, J. Rysä, O. Tenhunen, S. Ylä-Herttuala, et al., Vascular endothelial growth factor-b gene transfer prevents angiotensin II-induced diastolic dysfunction via proliferation and capillary dilatation in rats, Cardiovasc. Res. 89 (2011) 204–213.
[19] X.X. Shuai, Y.D. Meng, Y.X. Lu, G.H. Su, X.F. Tao, J. Han, et al., Relaxin-2 improves diastolic function of pressure-overloaded rats via phospholamban by activating Akt, Int. J. Cardiol. 218 (2016) 305–311.
[20] B. Chen, D. Lu, Y. Fu, J. Zhang, X. Huang, S. Cao, et al., Olmesartan prevents cardiac rupture in mice with myocardial infarction by modulating growth differentiation factor 15 and P53, Br. J. Pharmacol. 171 (2014) 3741–3753.
[21] E. Gao, Y.H. Lei, X. Shang, Z.M. Huang, L. Zuo, M. Boucher, et al., A novel and efficient model of coronary artery ligation and myocardial infarction in the mouse, Circ. Res. 107 (2010) 1445–1453.
[22] E. Gao, W.J. Koch, A novel and efficient model of coronary artery ligation in the mouse, Methods Mol. Biol. 1037 (2013) 299–311.
[23] S.F. Ehrentraut, V.F. Curtis, R.X. Wang, B.J. Saeedi, H. Ehrentraut, J.C. Onyiah, et al., Perturbation of neddylation-dependent NF-κB responses in the intestinal epithelium drives apoptosis and inhibits resolution of mucosal inflammation, Mol. Biol. Cell 27 (2016) 3687–3694.
[24] C. Lee, W. Yang, R.G. Parr, Development of the colle-salvetti correlation-energy formula into a functional of the electron density, Phys. Rev. B Condens. Matter 37 (1988) 785–789.
[25] A.D. Becke, Density-functional thermochemistry. III. The role of exact exchange, J. Chem. Phys. 98 (1993) 5648–5652.
[26] B. Miehlich, A. Savin, H. Stoll, H. Preuss, Results obtained with the correlation energy density functionals of becke and lee, yang and parr, Chem. Phys. Lett. 157 (1989) 200–206.
[27] S. Kandala, I.M. Kim, H. Su, Neddylation and deneddylation in cardiac biology, Am J Cardiovasc Dis 4 (2014) 140–158.
[28] S. Yu, L. Xie, Z. Liu, C. Li, Y. Liang, MLN4924 exerts a neuroprotective effect against oxidative stress via Sirt1 in spinal cord ischemia-reperfusion injury, Oxid Med Cell Longev 2019 (2019) 7283639.
[29] A.C. Andérica-Romero, J. Hernández-Damián, G.I. Vázquez-Cervantes, I. Torres, I. G. González-Herrera, J. Pedraza-Chaverri, The MLN4924 inhibitor exerts a neuroprotective effect against oxidative stress injury via Nrf2 protein accumulation, Redox Biol 8 (2016) 341–347.
[30] H. Su, J. Li, S. Menon, J. Liu, A.R. Kumarapeli, N. Wei, et al., Perturbation of Cullin deneddylation via conditional Csn8 ablation impairs the ubiquitin-proteasome system and causes cardiomyocyte necrosis and dilated cardiomyopathy in mice, Circ. Res. 108 (2011) 40–50.
[31] J. Zou, W. Ma, J. Li, R. Littlejohn, H. Zhou, I.M. Kim, et al., Neddylation mediates ventricular chamber maturation through repression of Hippo signaling, Proc. Natl. Acad. Sci. U. S. A. 115 (2018) 4101–4110.
[32] H. Su, J. Li, H. Osinska, F. Li, J. Robbins, J. Liu, et al., The Cop9 signalosome is required for autophagy, proteasome-mediated proteolysis, and cardiomyocyte survival in adult mice, Circ Heart Fail 6 (2013) 1049–1057.
[33] A. Kuma, M. Hatano, M. Matsui, A. Yamamoto, H. Nakaya, T. Yoshimori, et al., The role of autophagy during the early neonatal starvation period, Nature 432 (2004) 1032–1036.
[34] Y. Matsui, H. Takagi, X. Qu, M. Abdellatif, H. Sakoda, T. Asano, et al., Distinct roles of autophagy in the heart during ischemia and reperfusion: roles of Amp-activated protein kinase and Beclin 1 in mediating autophagy, Circ. Res. 100 (2007) 914–922.
[35] D. Gozuacik, A. Kimchi, Autophagy and cell death, Curr. Top. Dev. Biol. 78 (2007) 217–245.
[36] G. He, Y. Ma, Y. Zhu, L. Yong, X. Liu, P. Wang, et al., Cross talk between autophagy and apoptosis contributes to zno nanoparticle-induced human osteosarcoma cell death, Adv Healthc Mater 7 (2018), e1800332.
[37] K. Nishida, O. Yamaguchi, K. Otsu, Crosstalk between autophagy and apoptosis in heart disease, Circ. Res. 103 (2008) 343–351.
[38] V. Nikoletopoulou, M. Markaki, K. Palikaras, N. Tavernarakis, Crosstalk between apoptosis, necrosis and autophagy, Biochim. Biophys. Acta 1833 (2013) 3448–3459.
[39] J. Liu, Z.N. Guo, X.L. Yan, S. Huang, J.X. Ren, Y. Luo, et al., Crosstalk between autophagy and ferroptosis and its putative role in ischemic stroke, Front. Cell. Neurosci. 14 (2020) 577403.
[40] A. Hamacher-Brady, N.R. Brady, S.E. Logue, M.R. Sayen, M. Jinno, L. A. Kirshenbaum, et al., Response to myocardial ischemia/reperfusion injury involves bnip3 and autophagy, Cell Death Differ. 14 (2007) 146–157.
[41] D. Cui, D. Sun, X. Wang, L. Yi, E. Kulikowicz, M. Reyes, et al., Impaired autophagosome clearance contributes to neuronal death in a piglet model of neonatal hypoxic-ischemic encephalopathy, Cell Death Dis. 8 (2017) 2919.
[42] Y. Zhong, P. Zhong, S. He, Y. Zhang, L. Tang, Y. Ling, et al., Trimetazidine protects cardiomyocytes against hypoxia/reoxygenation injury by promoting amp-activated protein kinase-dependent autophagic flux, J. Cardiovasc. Pharmacol. 69 (2017) 389–397.
[43] F. Ng, B.L. Tang, Sirtuins' modulation of autophagy, J. Cell. Physiol. 228 (2013) 2262–2270.
[44] R. Garva, C. Thepmalee, U. Yasamut, S. Sudsaward, A. Guazzelli, R. Rajendran, et al., Sirtuin family members selectively regulate autophagy in osteosarcoma and mesothelioma cells in response to cellular stress, Front Oncol 9 (2019) 949.
[45] C.Y. Liu, Y. Zhou, T. Chen, J.C. Lei, X.J. Jiang, Ampk/Sirt1 pathway is involved in arctigenin-mediated protective effects against myocardial ischemia-reperfusion injury, Front. Pharmacol. 11 (2020) 616813.
[46] J.X. Wei, H.P. Xu, W. Zhen, Research progress of Sirt1 regulating autophagy in myocardial ischemia-reperfusion injury, Journal of Binzhou Medical University 43 (2021) 461–464.
[47] N. Hariharan, Y. Maejima, J. Nakae, J. Paik, R.A. Depinho, J. Sadoshima, Deacetylation of FoxO by Sirt1 plays an essential role in mediating starvation-induced autophagy in cardiac myocytes, Circ. Res. 107 (2010) 1470–1482.
[48] X. Wang, B. Wang, W. Gao, Y. An, G. Dong, J. Jia, et al., Helicobacter pylori inhibits autophagic flux and promotes its intracellular survival and colonization by down-regulating Sirt1, J. Cell Mol. Med. 25 (2021) 3348–3360.
[49] H. Zhang, X. Yang, X. Pang, Z. Zhao, H. Yu, H. Zhou, Genistein protects against ox-ldl-induced senescence through enhancing Sirt1/LKB1/AMPK -mediated autophagy flux in huvecs, Mol. Cell. Biochem. 455 (2019) 127–134.
[50] H. Wei, M. Yin, Y. Lu, Y. Yang, B. Li, X.X. Liao, et al., Mild hypothermia improves neurological outcome in mice after cardiopulmonary resuscitation through silent information regulator 1-actviated autophagy, Cell Death Dis. 5 (2019) 129.
[51] G. Luo, Z. Jian, Y. Zhu, Y. Zhu, B. Chen, R. Ma, et al., Sirt1 promotes autophagy and inhibits apoptosis to protect cardiomyocytes from hypoxic stress, Int. J. Mol. Med. 43 (2019) 2033–2043.
[52] Y.H. Wang, S.A. Li, C.H. Huang, H.H. Su, Y.H. Chen, J.T. Chang, et al., Sirt1 activation by post-ischemic treatment with lumbrokinase protects against myocardial ischemia-reperfusion injury, Front. Pharmacol. 9 (2018) 636.

[53] S.Y. Li, H.B. Su, The role of ubiquitin-like modification of neddylation in cardiac biology, Guangxi Sci. 25 (2018) 262–268.
[54] D. Cui, X. Xiong, Y. Zhao, Cullin-ring ligases in regulation of autophagy, Cell Div. 11 (2016) 8.
[55] G. Lu, L. Wang, J. Zhou, W. Liu, H.M. Shen, A destiny for degradation: interplay between Cullin-RING E3 ligases and autophagy, Trends Cell Biol. 31 (2021) 432–444.
[56] B. Samarasinghe, C.T. Wales, F.R. Taylor, A.T. Jacobs, Heat shock factor 1 confers resistance to Hsp90 inhibitors through p62/SQSTM1 expression and promotion of autophagic flux, Biochem. Pharmacol. 87 (2014) 445–455.
[57] L. Guan, Z. Yu, Z. Che, H. Zhang, M. Yu, Autophagic flux impairment exacerbates myocardial ischemia-reperfusion injury in experimental diabetes through Atg5/LAMP2 cleavage by calpains, Research Square (2020), https://doi.org/10.21203/rs.3.rs-42392/v1.
[58] S. Luo, D.C. Rubinsztein, Atg5 and Bcl-2 provide novel insights into the interplay between apoptosis and autophagy, Cell Death Differ. 14 (2007) 1247–1250.